Pergamon

Int. J. Heat Mass Transfer. Vol. 40, No. 14, pp. 3255–3266, 1997

Printed in Great Britain
0017–9310/97 $17.00+0.00

PII: S0017-9310(96)00385-7

Experimental investigation of mass transfer in a grid-generated turbulent flow using combined optical methods

F. LEMOINE, M. WOLFF and M. LEBOUCHÉ

LEMTA, 2, Avenue de la Forêt de Haye, BP 160, F-54504 Vandoeuvre-les-Nancy Cedex, France

(*Received* 26 *February* 1996 *and in final form* 15 *November* 1996)

Abstract—The aim of this paper is to provide some significant experimental results for the mass diffusion process from a point source in a quasi-isotropic homogeneous turbulent field generated by means of a grid. Experimental data for the mean, the fluctuating concentration fields, and the turbulent mass flux, which is the cross-correlation between concentration and velocity, are provided. Two combined optical non-intrusive methods, laser-induced fluorescence and laser Doppler velocimetry, have been used to measure simultaneously and instantaneously the concentration of the passive contaminant and the velocity of the flow. The experimental results are compared with a theoretical development, including the concept of turbulent diffusivity. An experimental determination of the turbulent diffusivity is also performed. © 1997 Elsevier Science Ltd.

1. INTRODUCTION

The understanding of the diffusion process of a passive contaminant in turbulent flows appears to be critical in many fundamental and industrial investigations. Turbulent characteristics of the flow field strongly affect the mass transfer properties. The importance of the turbulent diffusion phenomena can be found in many physical processes, e.g. the spread of a polluant, or the mixing processes in chemical reactions. Mass transfer phenomena are also expected to share common characteristics with heat diffusion; it also contributed to the understanding of heat transfer and the design of heat exchangers.

The diffusion of a passive contaminant (concentration C), under turbulent conditions, can be described by [1]

$$\overline{U_i}\frac{\partial \bar{C}}{\partial x_i} = \frac{\partial}{\partial x_i}\left(\sigma\frac{\partial \bar{C}}{\partial x_i} - \overline{u_i c}\right) \quad (1)$$

where the concentration and velocity are separated into the mean and the fluctuating part ($U_i = \overline{U_i} + u_i$, $C = \bar{C} + c$), and σ is the molecular diffusivity.

The determination of the diffusion field of a transferable passive contaminant involves the knowledge of the turbulent mass flux. This mass flux, transported by turbulence, corresponds to the cross-correlation between concentration and velocity fluctuations, and this term needs to be measured accurately. An experimental technique is developed which is able to characterize this term. Optical techniques are appropriate, because the sample volume is compatible with the turbulent scales being measured, and they are non-intrusive. In the present paper, one investigates the turbulent diffusion of a passive contaminant, issuing from a continuous point source in a quasi-isotropic homogeneous water turbulent flow. Quasi-isotropy and homogeneity are generated by means of a grid.

Various techniques have been implemented to measure the turbulent mass or temperature flux. One of these techniques was based on the light-scattering properties of solid particles, whose concentration was measured in the flow field. Rosensweig *et al.* [2] pioneered this kind of measurement, and Shaughnessy and Morton [3] measured the particle concentration in a turbulent jet, using light scattering. However, these measurements provided the particle concentration and not the molecular concentration. Kotsovinos [4] combined one-dimensional laser Doppler velocimetry (LDV) with fast response thermistors to measure simultaneously the fluctuations of a scalar and the velocity. The difficulty was to adjust the measurement volume of the velocimeter and the temperature probe, which can cause a biased calculation of the correlation. Chevray and Tutu [5] performed simultaneous temperature and velocity measurements by means of two hot wires, and obtained the cross-correlation between temperature and velocity in a turbulent jet. Dibble *et al.* [6] obtained simultaneous measurements of passive scalars (concentration and temperature) and velocity in a turbulent flame, by means of combined LDV and vibrational laser Raman scattering. However, this set-up was designed for the determination of concentration–velocity and temperature–velocity cross-correlations under extreme conditions, such as in flames and combustion, and the experimental apparatus seems to be quite complicated to implement. Owen [7] was the first to implement simultaneous laser velocimetry and laser-induced flu-

NOMENCLATURE

C	molecular concentration
C_c	centerline molecular concentration
D_t	turbulent diffusivity
k	kinetic energy
M	grid mesh
N	sample number
P	pressure
(r, θ, x)	cylindrical coordinates
r_c	concentration profile half-width radius
r_{cor}	cross-correlation profile half-width radius
R_{ij}	Reynolds stress tensor
S_f	fluorescence signal
U_i	velocity component in the ith direction
U	axial velocity component
V	radial velocity component
x_i	cartesian coordinates.

Greek symbols

ε	kinetic energy dissipation rate
ν	kinematic viscosity
ρ	density
σ	molecular diffusivity.

Other symbols

*	normalized values
X	instantaneous values of X
$\bar{X}$	mean value of X
x	fluctuating part of X.

orescence measurements, in order to investigate the mixing of coaxial jets. Papanicolaou and List [8] studied turbulent buoyant jets by means of a combined LDV and laser-induced fluorescence (LIF) system: a measurement of the turbulent mass flux profile in the jet was provided. An experimental determination of the turbulent mass flux and the turbulent diffusivity has been performed in a turbulent submerged jet by Lemoine *et al.* [9], by combining LIF of rhodamine B and LDV. The experimental set-up which has been used was very simple to implement. If the literature is very dense about investigations of the turbulent mass or temperature fluxes in jets and shear flows, it appears very poor about experimental studies of the turbulent diffusion process in isotropic turbulence fields, e.g. grid-generated turbulence flow. Gad-el-Hak and Morton [10] attempted to determine the concentration–velocity cross-correlation by means of a combined LDV and light-scattering technique, but the experimental results were too scattered to be significant. Simoens and Ayrault [11] studied the jet of a passive contaminant submerged in an isotropic homogeneous turbulent channel by using two combined imaging techniques: particle image velocimetry and planar LIF. Considerable work has been done by Nakamura *et al.* [12] on mass diffusion in grid-generated turbulence. In this article, concerning the experimental apparatus, the emphasis is layed on the reduction of the wake and the perturbations due to the injection device. The velocity fluctuations are measured by means of hot films, and concentration using a light absorption technique. Accurate results of the mean and fluctuating concentration fields are reported. Also provided is a theoretical development of the cross-correlation between concentration and velocity, under quasi-isotropic and homogeneous turbulent conditions. However, the available measurements are not sufficient to allow a comparison.

The aim of the present paper is to provide non-intrusive measurements of the diffusion field of a passive contaminant in grid-generated turbulence. The mean concentration field and the fluctuating concentration and velocity fields will be provided as a first step. The second step concerns the turbulent mass flux. The cross-correlation between the concentration and velocity fluctuations has been measured, and a reduced profile of this parameter has been determined. The turbulent diffusivity has also been determined, and the experimental results will be compared with theoretical concepts.

2. EXPERIMENTAL ARRANGEMENT

2.1. *Measurement set-up: combined concentration and velocity measurements*

The concentration has been measured using LIF of an organic dye, which is the passive contaminant. The fluorescence phenomenon and its modelization has been detailed in refs. [13, 14]. The passive contaminant here is an organic fluorescent dye. If the concentration of the dye is low enough, the attenuation of the laser beam and fluorescence signal in the absorbing medium can be neglected [9]. As a consequence, the measured fluorescence signal turns out to be directly proportional to the concentration:

$$S_f = K_{opt} V_c L_0 \Phi \varepsilon_1 C \qquad (2)$$

where K_{opt} is an optical constant, V_c is the collection volume, I_0 is the incident laser beam intensity, Φ is the fluorescence quantum yield, and C is the molecular concentration. The frequency response of the fluorescence is very high, exceeding 10^6 Hz.

The properties of rhodamine B ($C_{28}H_{31}ClN_2O_3$), an organic dye, are appropriate for performing concentration measurements by LIF. This dye is highly soluble in water, and its fluorescence, centered on the red–orange part of the visible spectrum, is strong. The

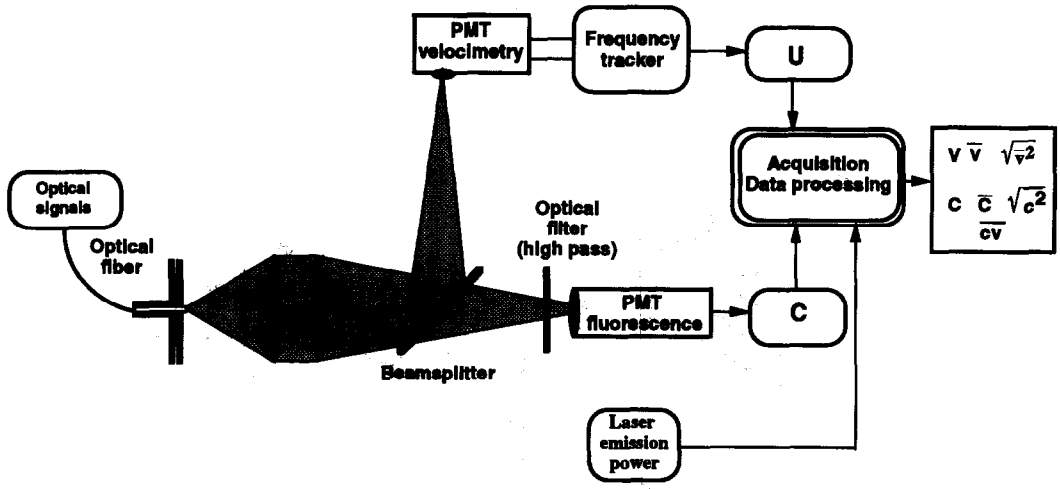

Fig. 1. Optical arrangement.

fluorescence of this dye can be induced by the green line of an argon laser ($\lambda = 514.5$ nm), commonly available in laboratories.

The concentration measurement using LIF has been combined with the velocity measurement by a laser Doppler velocimeter (Fig. 1). The main component of the optical set-up is a laser Doppler velocimeter, which is equipped with an argon-ion laser tuned to the green line ($\lambda = 514.5$ nm) and a frequency shifter unit. In the present experiment, the forward scattering configuration has been used. The probe volume for both the laser-induced fluorescence and the laser velocimetry measurements is the intersection point of the two laser beams. The dimensions of the measurement volume are about 250 μm along the transverse axis, and 20 μm along the longitudinal axis. The collection device which is connected to the laser beam guiding system is mounted on a three-dimensional traversing device to keep the probe volume continuously focused. Two kinds of signals are emitted from the probe volume. One is the Doppler signal, and the other is the fluorescence of rhodamine B, emitted at higher wavelengths than the former. The same optics collects both the Doppler and the fluorescence signals. These signals are subsequently separated and processed. A part of the optical signal is processed by a photomultiplier, connected to a frequency tracker to yield the velocity and its fluctuations. The second part first passes through a high-pass filter to eliminate the frequency resulting from the Mie scattering from particles due to the incident laser radiation, and is then detected by a second photomultiplier, to provide the fluorescence signal, which is proportional to the concentration. The present device allows one to obtain simultaneously, and, at the same point, the concentration and velocity. This is a condition which avoids the spatial bias in the calculation of the concentration-velocity cross-correlations.

Although the laboratory room was darkened, it appeared necessary to measure the optical noise, including the residual daylight and any unblocked laser radiation. This noise is then subtracted from the fluorescence signal, and the difference is normalized by the laser output power. The data, such as the analog Doppler and fluorescence signal, are transmitted to a computerized acquisition board, where they are sampled and processed. Subsequently, the mean, rms and cross-correlation values of the velocity and concentration are calculated.

The accuracy of the technique has been checked: the accuracy of the concentration measurement is about 3%, and the accuracy of the velocity measurement is about 2%.

2.2. *Flow conditions*

The present experiments are performed in a 60 mm square test channel, which is equipped with two optical windows, one for laser beam access and the other for signal detection (Fig. 2). A squared grid is implanted in the test channel. The characteristics of the grid are a 1 cm mesh, denoted by M, and a 1 mm bar thickness. An injection device, which consists of a cylindrical round nozzle, is positioned 50 mm downstream of the grid. The nozzle is able to supply a dye solution, whose velocity can be adjusted by means of a nitrogen counter-pressure.

In the first step, the decrease in the concentration from 0 to 20 mm downstream of the nozzle exit is measured. The rate of decrease of the concentration was about 30. The measurements performed close to the nozzle exit are not acceptable, due to perturbations of the injection device, and also because the grid turbulence field is not entirely well established. As a result, the first measurements are performed 20 mm downstream of the nozzle exit.

A concentration of rhodamine B of 2×10^{-7} mol l^{-1} is required to reach the conditions under which the fluorescence signal is proportional to the concentration. This concentration has been selected as a trade-off between the attenuation of the incident laser

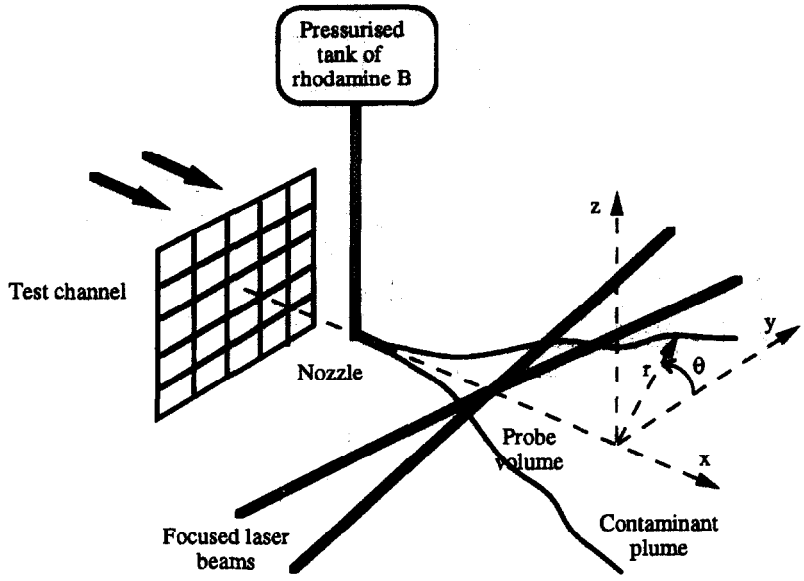

Fig. 2. Experimental arrangement.

beam along the absorbing medium and the signal level, which must remain acceptable. By considering the rate of decrease between the nozzle exit and the first measurement section ($x = 20$ mm downstream of the grid), the selected dye concentration at the injection point was 6×10^{-6} mol l^{-1}. The concentration of the dye will be 2×10^{-7} mol l^{-1} or less in the first measurement section. The mean velocity of the flow channel is about 1.7 m s^{-1}. The injection velocity at the nozzle exit is adjusted by means of a nitrogen counter-pressure at the same value in order to avoid, if possible, the shear effects between the grid-generated turbulence flow and the contaminant plume. To define the velocity field, cartesian coordinates have been used: x is the axial direction along the nozzle axis, and y and z are the transverse coordinates. The axial velocity component is denoted by $U(U = \bar{U}+u)$ and the transverse component in the z-direction (see Fig. 2) by $V(V = \bar{V}+v)$.

3. EXPERIMENTAL RESULTS OF MEAN AND FLUCTUATING FIELDS

3.1. *Mean concentration field*

Numerous results have been published for the concentration field downstream of a jet [3, 9]. Only a few results concerning the spread of a concentration plume in a grid-generated turbulence flow are available [10–12]. In the case of isotropic turbulence, the theory predicts that the mean concentration field downstream of the grid is Gaussian [1, 12]. The grid turbulence is well established for $x/M = 20$; however, turbulent diffusion of the concentration in the turbulent field can be analysed for $x/M = 10$.

The concentration along the nozzle axis, from $x/M = 7$ to $x/M = 23$ (M denotes the mesh of the grid) was investigated first. The rate of decrease of the concentration is about 7 (Fig. 3). The inverse of the concentration ($1/C$) grows linearly with the reduced downstream position x/M. A significant change of slope is observed for $x/M = 10$. This phenomenon shows the influence of the wake of the injection device on the scalar field. As a consequence, the concentration $C_c(x)$ along the jet axis follows a hyperbolic law (Fig. 3):

$$\frac{1}{C_c(x)} = 1.27\frac{x}{M} - 0.94. \tag{3}$$

This result is congruent with the slope of the distribution of $1/C$ along the contaminant plume found by Nakamura *et al.* [12].

The radial profiles of the mean concentration are measured at various locations downstream of the grid in the vertical and horizontal directions (z and y, respectively), and are shown in Fig. 4 for the y-direction. The data have been obtained at various downstream locations ($x/M = 10, 13, 15, 17, 18, 20, 22$). Since the concentration plume is axisymmetric, cylindrical coordinates (r, θ, x) will also be used. The concentration was normalized by the concentration of the nozzle axis $C_c(x)$, and the radial distance r by the half-width radius, r_c, of the mean concentration profile. The reduced mean concentration profiles have a similar shape, following a Gaussian law:

$$\frac{C(x)}{C_c(x)} = e^{-\ln 2(r/r_c)^2}. \tag{4}$$

The data reported in Table 1 show that the concentration profiles in the y-direction are larger than in the z-direction. This non-axisymmetric concentration field is caused by the disturbance of the injection

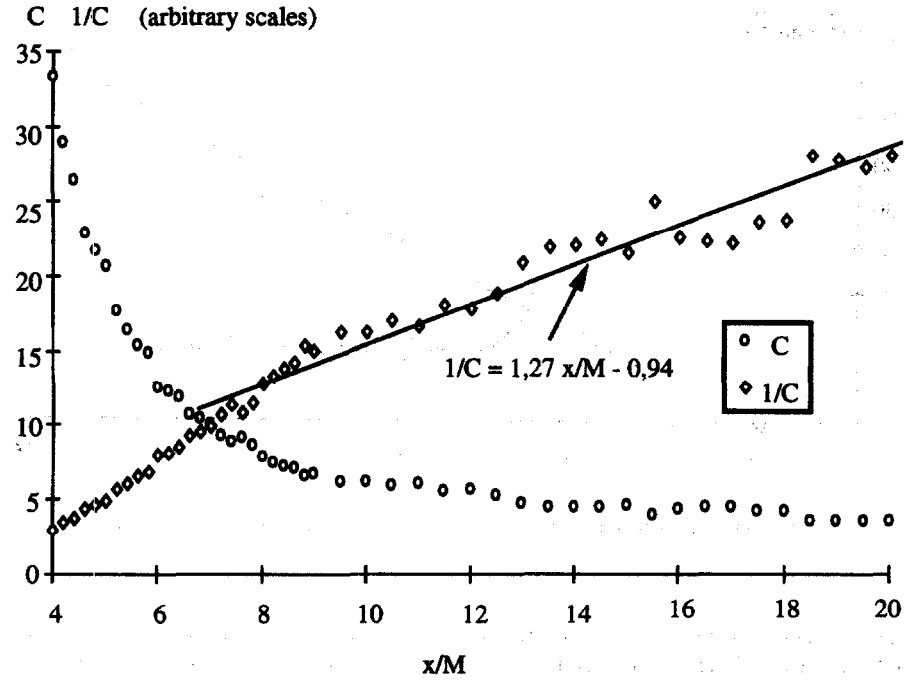

Fig. 3. Concentration behaviour along the nozzle axis.

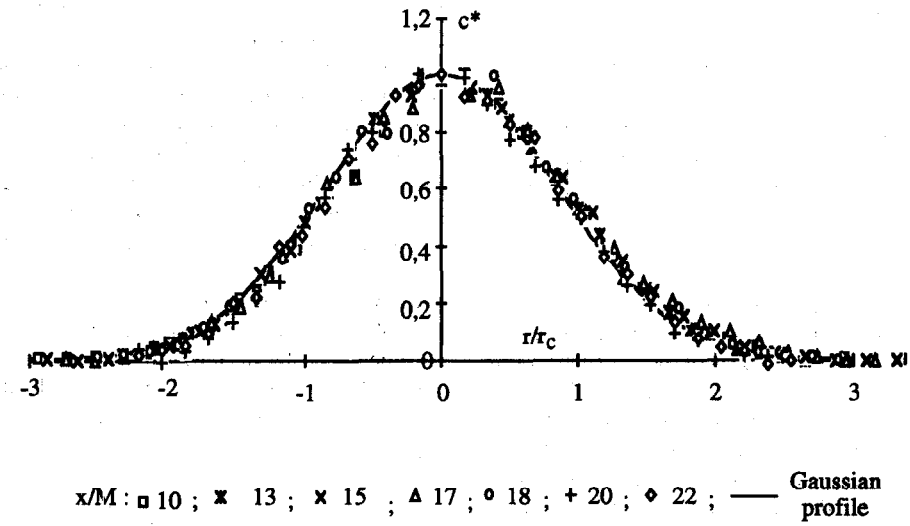

Fig. 4. Reduced profiles of dye concentration (obtained along the y-direction).

device, which generates an inhomogeneity in the turbulent field. The degree of inhomogeneity can be estimated by [12]

$$\frac{\overline{v_y^2}^{1/2}}{\overline{v_z^2}^{1/2}} = \frac{r_{cy}}{r_{cz}} \tag{5}$$

where $\overline{v_y^2}$ and $\overline{v_z^2}$ are the rms values of the transverse velocity along the y- and z-directions, and r_{cy} and r_{cz} are the half-width radius of the concentration in both directions. For $x/M' \geqslant 15$, $r_{cy}/r_{cz} = 1.38$ and

$$\frac{\overline{v_y^2}^{1/2}}{\overline{v_z^2}^{1/2}} = 1.36$$

(see also Table 1).

The experimental data seem to be reliable, since the reduced profiles are self-similar and Gaussian, which is consistent with the theoretical predictions for a point source of contaminant in an isotropic turbulence [1, 12].

The growth of the dispersion length scale of the

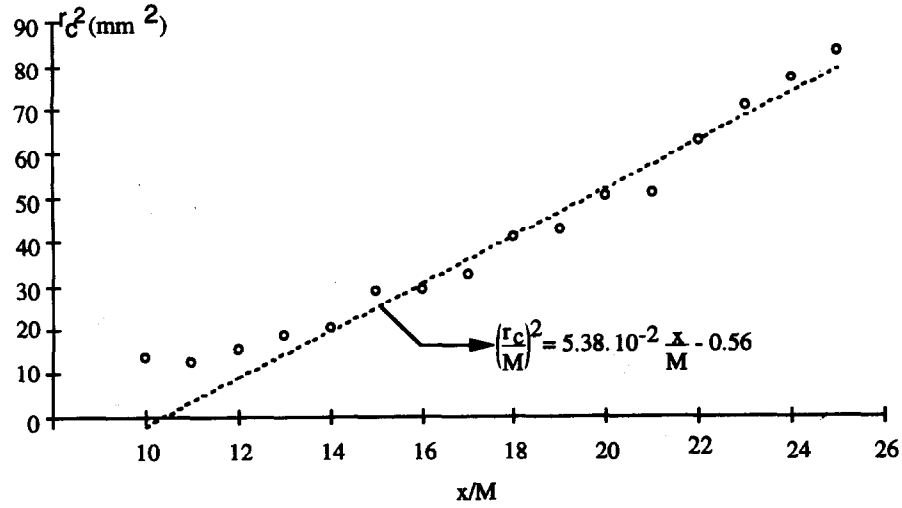

Fig. 5. Downstream evolution of the half-width radius r_c of the concentration profile.

concentration, characterized by the half-width radius r_c, has been determined in 16 cross-sections, to obtain a reliable evolution. The half-width radius grows linearly, from $x/M = 13$, with the square root of the distance from the grid (Fig. 5), as expected theoretically [1, 12].

It follows that

$$\left(\frac{r_c}{M}\right)^2(x) = 5.38 \times 10^{-2}\frac{x}{M} - 0.56. \qquad (6)$$

Between $x/M = 10$ and $x/M = 13$, the concentration dispersion length scale does not follow the general trend, since the homogeneous turbulence is not well established.

3.2. *Fluctuating field*

The experimental apparatus allows one to record simultaneously, and in the same sample volume, concentration and velocity fluctuations. The rms values of the velocity and concentration fluctuations have been recorded simultaneously in locations where the mean concentration has been measured. The rms value of the components of the velocity fluctuations is normalized by the mean flow velocity $\bar{U}$, and are presented as a function of the radial distance in Fig. 6. The effects of the injection device can be observed from the nozzle exit to $x/M = 10$. Downstream of the location $x/M = 13$, rms fluctuation profiles of the velocity U and V_y appear as homogeneous along the diameter. A significant perturbation in the fluctuating field of the V_z-component, caused by the injection pipe, in the vicinity of the centerline, can be observed in all of the investigated zone. The rms values of the components of the velocity present the same order of magnitude, but are not equal: the longitudinal velocity component fluctuations are higher than the two transverse ones, along the two directions, since turbulence production is greater in the longitudinal direction. Isotropy cannot be realized in such a test channel, where a contraction would be required [16]. The fluctuation rate of the longitudinal velocity in the self-preserving zone decreases from 6.5% at $x/M = 13$ to 5.5% at $x/M = 20$. One significant point in grid turbulence is the decrease in the inverse of the turbulent fluctuations of longitudinal velocity [1, 15]. This decrease is shown in Fig. 7, and can be adequately represented by a power law:

$$\frac{\bar{U}}{\overline{u^2}} = 3.98\left(\frac{x}{M} - 2\right)^{1.25}. \qquad (7)$$

Table 1. Measured parameters in the cross-section for $10 \leqslant x/M \leqslant 22$

x/M	r_{cz} [mm]	r_{cy} [mm]	r_{cy}/r_{cz}	$\overline{v_z^2}^{1/2}$	$\overline{v_y^2}^{1/2}$	$\frac{\overline{v_y^2}^{1/2}}{\overline{v_z^2}^{1/2}}$	r_{cor} [mm]	$K = r_{cor}/r_{cz}$
10	3.65	3.74	1.1	0.042	0.067	1.6	5.70	1.56
13	3.9	4.93	1.26	0.04	0.060	1.53	6.9	1.77
15	5.35	7.26	1.35	0.038	0.053	1.38	8.45	1.57
17	5.7	8.36	1.47	0.036	0.049	1.34	8.65	1.52
18	6.4	8.77	1.37	0.035	0.047	1.35	10.65	1.67
20	7.1	9.71	1.37	0.034	0.046	1.36	10.55	1.50
22	7.9	10.07	1.35	0.033	0.044	1.32	11	1.57

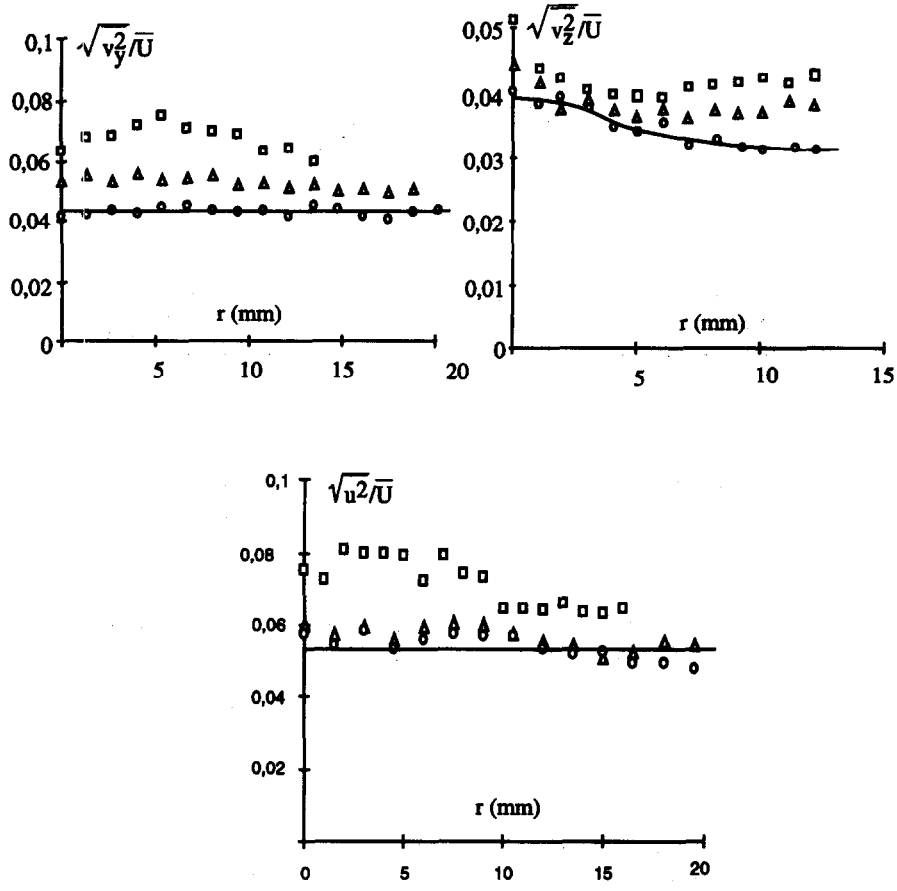

Fig. 6. Distribution of the transverse and longitudinal velocity fluctuation rates in various cross-sections (transverse velocity fluctuation rates are given along the y- and z-directions).

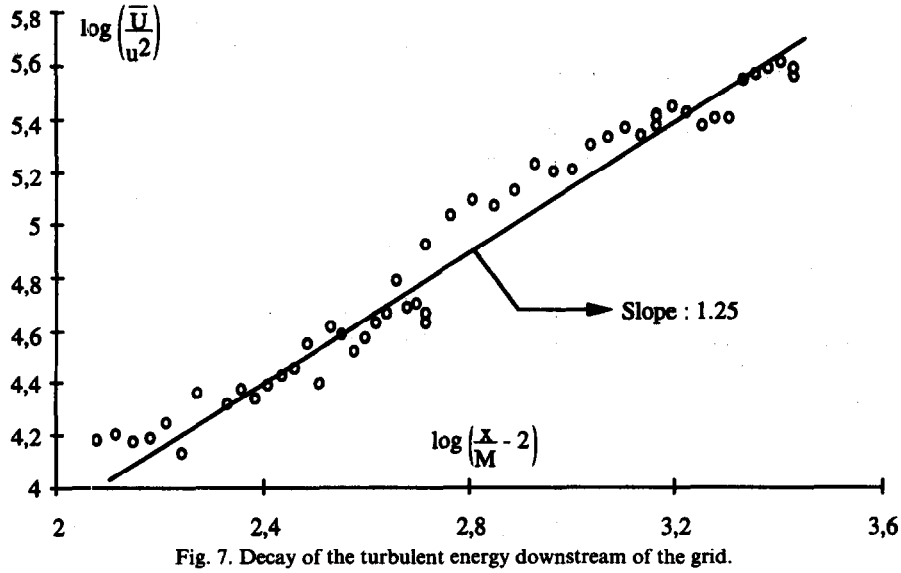

Fig. 7. Decay of the turbulent energy downstream of the grid.

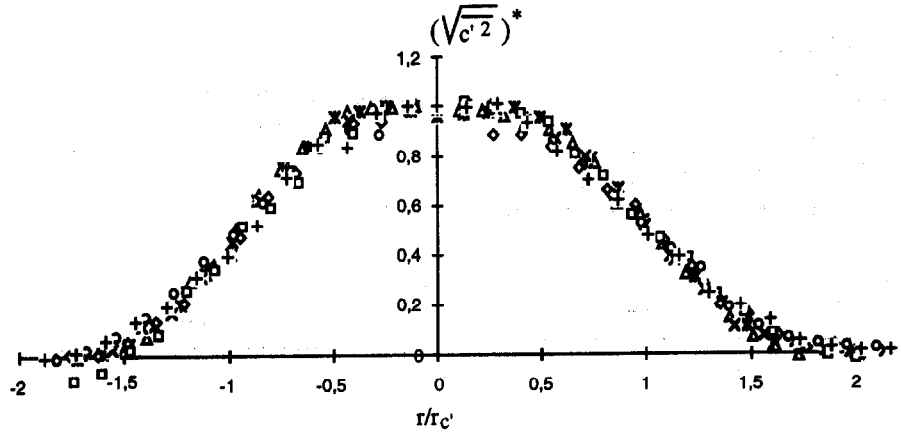

x/M : ✖ 10 ; ▲ 13 ; ✖ 15 ; + 17 ; ○ 18 ; ◇ 20 ; □ 22

Fig. 8. Reduced profile of the concentration fluctuations (obtained along the y-direction).

This power law appears to be in agreement with the results found by Comte-Bellot and Corsin [16].

Under quasi-isotropic turbulent conditions, the energy dissipation rate ε can be evaluated by

$$\varepsilon = -\frac{3}{2}U\frac{d\overline{u^2}}{dx} \approx 80\left(\frac{x}{M}-2\right)^{-2.25}. \quad (8)$$

The rms values of the concentration fluctuations have been scaled by the local rms value on the nozzle axis, and the radial distance by the half-width radius of the rms concentration profiles. A self-similarity between the reduced rms of concentration profiles at different cross-sections of the flow has been pointed out (Fig. 8), which is congruent with the results obtained by Nakamura *et al.* [12].

4. TURBULENT TRANSPORT

4.1. *Theoretical concepts*

The problem is axisymmetric: the (r, θ, x) cylindrical coordinate system has been used. The molecular diffusion phenomena are neglected, compared to diffusion by turbulence [17]. The fundamental equation of the turbulent mass transport, for the present problem, can be written by using a boundary layer approximation [12]:

$$U\frac{\partial \bar{C}}{\partial x} = -\frac{1}{r}\frac{\partial}{\partial r}(r\overline{vc}). \quad (9)$$

The term $\overline{vc}$ is unknown: a closure is required.

The general equation governing the transport of the turbulent concentration flux $\overline{u_i c}$ (here $\overline{uc}$ and $\overline{vc}$), can be written as [18]

$$\frac{\partial \overline{u_i c}}{\partial t} + \overline{U_j}\frac{\partial \overline{u_i c}}{\partial x_j} = -R_{ij}\frac{\partial \bar{C}}{\partial x_j} - \overline{u_i c}\frac{\partial \overline{U_j}}{\partial x_j} - \frac{\overline{c}}{\rho}\frac{\overline{\partial p}}{\partial x_i} - \frac{\partial \overline{u_i u_j c}}{\partial x_j} + \sigma\frac{\overline{u_i \partial^2 c}}{\partial x_j^2} + v\frac{\overline{c\partial^2 u_i}}{\partial x_j^2} \quad (10)$$

where P is the static pressure ($P = \bar{P}+p$), R_{ij} is the Reynolds stress tensor, σ is the molecular diffusivity, and v is the kinematic viscosity.

Assuming that the flow field and turbulence are homogeneous, and neglecting the molecular diffusion and dissipation terms, equation (10) can be rewritten, using the polar coordinate, in the radial direction:

$$U\frac{\partial \overline{vc}}{\partial x} = -\frac{\overline{c}}{\rho}\frac{\overline{\partial p}}{\partial r} - \overline{v^2}\frac{\partial \bar{C}}{\partial r} - \frac{\partial \overline{v^2 c}}{\partial r}. \quad (11)$$

It can be assumed, as in the case for the $\overline{uv}$ component in a plane jet [19], that the convection and turbulent diffusion are much smaller than the pressure and production terms. Equation (11) reduces to equation (12).

The resulting equation is

$$\overline{v^2}\frac{\partial \bar{C}}{\partial r} \approx -\frac{\overline{c}}{\rho}\frac{\overline{\partial p}}{\partial r}. \quad (12)$$

The pressure scrambling term is usually associated with a tendency towards isotropy, and can be modelled as a relaxation term [equation (13)], of the form [18]

$$-\frac{\overline{c}}{\rho}\frac{\overline{\partial p}}{\partial r} \approx -\frac{\overline{p}}{\rho}\frac{\overline{\partial c}}{\partial r} = C_{c1}\frac{\varepsilon}{k}\overline{vc} \quad (13)$$

where C_{c1} is a constant, k is the turbulent kinetic energy, and ε is its dissipation rate.

Equations (12) and (13) show that the turbulent mass flux and the radial concentration gradient can be considered as proportional:

$$\overline{vc} \approx \overline{v^2}\frac{1}{C_{c1}}\frac{k}{\varepsilon}\frac{\partial \bar{C}}{\partial r}. \quad (14)$$

Usually, the proportionality constant defines the turbulent diffusivity, denoted by D_t. As a consequence, the following closure of equation (8) is used:

$$\overline{vc} = -D_t \frac{\partial \bar{C}}{\partial r}. \quad (15)$$

As shown in the present experiments, and in the literature [12], the concentration profile is assumed to follow a Gaussian law:

$$C = C_c(x)\, e^{\ln 2 (r/r_c)^2} = C_c(x) f(\zeta) \quad (16)$$

where $f(\zeta) = e^{-\ln 2 \zeta^2}$. ζ denotes the reduced radial coordinate ($\zeta = r/r_c$).

By considering the self-similarity assumption, the mass flux Φ is conserved in the self-preserving region:

$$\Phi = \bar{U} C_c(x) r_c^2(x) = \text{constant}. \quad (17)$$

According to equations (9), (15) and (17), the turbulent diffusivity D_t can be determined:

$$D_t = \frac{\bar{U}}{4 \ln 2} \frac{dr_c^2}{dx}. \quad (18)$$

D_t is a constant, since the evolution of r_c^2 is linear with x.

As a result, a theoretical profile of the concentration–velocity cross-correlation can be predicted. The $\overline{vc}$ profile is determined by equation (18). Assuming that the radial concentration profile is Gaussian, and using the radial reduced coordinate ζ, the $\overline{vc}$ profile is

$$\overline{vc}(x, \zeta) = -\bar{U} \frac{C_c(x)}{2 r_c(x)} \frac{dr_c^2(x)}{dx} \zeta f(\zeta)$$

$$= H(x) \zeta f(\zeta) \quad (19)$$

where $H(x)$ is a function which depends only on the axial coordinate x.

According to equation (19), the cross-correlation profiles are self-similar. The cross-correlation value can be normalized by its maximum value, and the radial distance by the half-width radius of the correlation profile, denoted by r_{cor}, defined by

$$\frac{\overline{vc(r_{cor})}}{(\overline{vc})_{max}} = \frac{1}{2}. \quad (20)$$

The maximum value of the cross-correlation profile is determined by

$$\frac{d\overline{vc}(x, \zeta)}{d\zeta} = 0$$

which gives

$$[\overline{vc}]_{max} = H(x) \sqrt{\frac{1}{2 \ln 2}} e^{-1/2}. \quad (21)$$

The half-width radius r_{cor} of the cross-correlation profile is given by the following equation:

$$\frac{r_{cor}}{r_c} e^{-\ln 2 r_{cor}^2 / r_c^2} = \frac{1}{2} \sqrt{\frac{1}{2 \ln 2}} e^{-1/2}. \quad (22)$$

It shows that ratio between the half-width radius of the correlation and the half-width radius of the concentration is a constant, K. The highest value of K, from equation (22), is 1.64. The characteristic radial distance for the correlation profile is $r_{cor} = 1.64 r_c$. As a consequence, the length scale of the turbulent mass flux r_{cor} grows linearly with the square root of the distance from the grid. As a result, the expression of the turbulent mass flux, reduced by its maximum value, denoted by $\overline{vc}^*$, as a function of the reduced distance ζ', is

$$\overline{vc}^*(\zeta') = \frac{K \zeta' e^{-\ln 2 K^2 \zeta'^2}}{\sqrt{\frac{1}{2 \ln 2}} e^{-1/2}} \quad \text{where } \zeta' = \frac{r}{r_{cor}}. \quad (23)$$

4.2. *Measurements of the cross-correlation profiles*

The concentration and velocity fluctuations were recorded simultaneously in the same probe volume. It allows one to obtain the unbiased cross-correlation between the concentration and velocity fluctuations. This term characterizes the flux of the matter, here the fluorescent tracer, transported by turbulence. This cross-correlation is practically derived from the formula

$$\overline{vc} = \frac{1}{N} \sum_{i=1}^{N} (V_i - \bar{V})(C_i - \bar{C}) \quad (24)$$

where i is the sampling index, and N is the number of samples. $\bar{V}$ is equal to zero.

The error in the evaluation of the cross-correlation function is limited to 1% for a number of samples $N \approx 50\,000$ [20]. Furthermore, the accuracy of the amplitude of the correlated signals has a small influence on the cross-correlation value.

After processing of the experimental data, one observes that the correlation profiles are similar for different cross-sections of the flow field. As predicted by the theory, the cross correlation is anti-symmetric. The correlation value is zero on the nozzle axis, has a maximum value away from the nozzle axis, and decreases to zero out of the contaminant plume. The correlation profiles have been reduced to determine the self-similarity law. The radial distance has been reduced by the half-width radius of the correlation profile. The value of the cross-correlation is normalized by its maximum value. Some values of the measured half width radius of correlation and concentration profiles are reported in Table 1. The ratio between these parameters, denoted by K, has also been calculated. K is almost constant in all of the investigated cross-sections, as predicted by equation (22). The averaged value of K is about 1.57, which is in agreement with the value determined theoretically ($K = 1.64$).

A profile of the reduced concentration–velocity cross-correlation $\overline{vc}^*(\zeta')$, measured in various cross-sections of the flow field, is shown in Fig. 9: the self-similarity predicted by the theory can be checked. Other authors have performed measurements of the

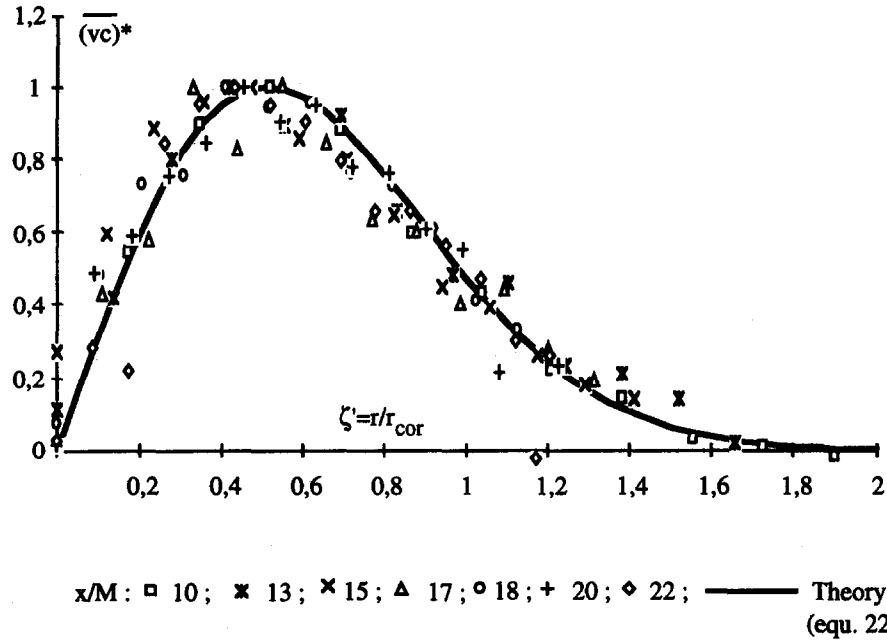

Fig. 9. Reduced profile of radial turbulent mass flux.

turbulent mass flux in quasi-similar conditions. Gad-el-Hak and Morton [10], by operating with a grid turbulent air flow, attempted to avoid the shear effects by performing measurements far downstream of the grid. The general trend of the obtained concentration–velocity cross-correlation profiles is congruent with the profiles found in the present work. However, the experimental data reported in the work of Gad-el-Hak and Morton are too scattered to be reliable and to be compared accurately. Also plotted in Fig. 9 is the theoretical shape of the reduced $\overline{vc}^*$ profile, which appears to be in full agreement with the reported experiments.

4.3. *Evaluation of the turbulent diffusivity*

As shown previously, the turbulent diffusivity can be determined by equation (15). It has been shown that both the concentration and the concentration–velocity cross-correlation profiles can be reduced. As a consequence, a reduced turbulent diffusivity, denoted by D_t^*, can be determined.

When the reduced radial coordinate ζ' is used, the reduced turbulent diffusivity can be written as

$$D_t^* = -\overline{vc}^*(\zeta') \Big/ \frac{\partial C^*(\zeta')}{\partial \zeta'} \tag{25}$$

where $\overline{vc}^*(\zeta')$ is the reduced measured correlation profile, expressed by the ζ' coordinate, and C^* is the reduced concentration profile.

As a result, the reduced turbulent diffusivity can be obtained from equations (16) and (25):

$$D_t^* = \frac{\overline{vc}^*(\zeta')}{2\zeta' \ln 2K^2 \, e^{-\ln 2K^2\zeta'^2}}. \tag{26}$$

The evolution of D_t^* as a function of ζ' is presented in Fig. 10. The values of D_t^* are very scattered for $|\zeta'| \leqslant 0.1$. For ζ' ranging from 0.1 to 1.5, the reduced turbulent diffusivity is almost constant for the different cross-sections. The mean value of the reduced turbulent diffusivity is about 0.84. For $|\zeta'| \geqslant 1.5$, the reduced turbulent diffusivity is highly scattered. This phenomenon can be attributed to an inaccuracy of the measurement of the correlation in a region where the fluorescence signal is very low, and where the signal–noise ratio is not acceptable.

The measured reduced turbulent diffusivity has also been compared to the theoretical one. According to the expression of the reduce correlation profile, the theoretical value of the turbulent diffusivity is

$$D_t^* = \frac{e^{1/2}}{2\sqrt{2\ln 2}} \frac{1}{K} \approx 1.41 \frac{1}{K}. \tag{27}$$

The theoretical value of D_t^* depends only on the ratio, K, between the characteristic radius of the correlation and concentration profiles. D_t^*, calculated by equation (27), is about 0.85, which is in full agreement with the value found experimentally.

5. CONCLUSION

In the present paper, some significant experimental results have been provided for the mass diffusion process from a point source in a grid-generated turbulent flow. The measurement technique that has been implemented is based on LIF combined with LDV. This technique allows one to obtain the mean and fluctuating concentration fields, and the turbulent

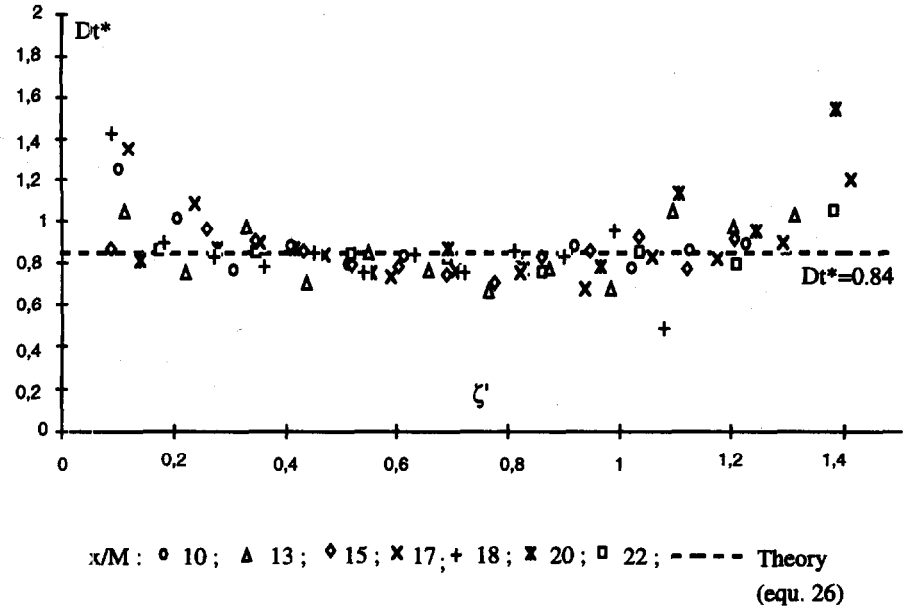

Fig. 10. Evaluation of the turbulent diffusivity (in normalized values).

mass flux, which corresponds to the concentration–velocity cross-correlation.

The mean and fluctuating concentration fields that have been determined are in full agreement with the results available in the literature, and with the theoretical predictions. The cross-correlation between the concentration and the velocity has also been measured; a self-similarity between the correlation profiles, measured in various cross-sections, has been pointed out. The turbulent mass flux has been investigated theoretically, assuming a boundary layer approximation. Theory and experiments are in full agreement. The theory has pointed out that the dispersion length scale of the concentration and turbulent mass flux, defined in this paper, are proportional. This particular point has been experimentally well checked. A turbulent diffusivity has also been determined, which is assumed to be a scalar under homogeneous turbulent conditions. The turbulent diffusivity is defined as the ratio between the turbulent mass flux and the radial concentration gradient. This turbulent diffusivity is almost constant along the radial coordinate.

The measurement of the turbulent mass flux appears very important in the understanding of the turbulent diffusion process. Some other terms present in the transport equation of the turbulent mass flux, such as the correlation $\overline{v^2 c}$ or the gradient $\partial \overline{vc}/\partial x$, could be measured in order to determine the pressure scrambling term $(c/\rho)(\partial p/\partial r)$. The general balance of the equation for $\overline{vc}$ could allow one to validate the turbulent diffusivity hypothesis. In future investigations, it would be also desirable to measure simultaneously the radial and axial components of the velocity, by means of a two-dimensional laser Doppler velocimeter, which could also be combined with a LIF technique. It would be possible to perform experimentally a comparison between the radial and axial turbulent mass fluxes, $\overline{uc}$ and $\overline{vc}$.

REFERENCES

1. Hinze, J. O., *Turbulence*. McGraw-Hill, New York, 1975.
2. Rosensweig, R. E., Hottel, H. C. and Williams, G. C., Smoke-scattered light measurement of turbulent concentration fluctuations. *Chemical Engineering Science*, 1961, **12**, 111–129.
3. Shaughnessy, E. G. and Morton, J. B., Laser light-scattering measurements of particle concentration in a turbulent jet. *Journal of Fluid Mechanics*, 1977, **80**, 129–148.
4. Kotsovinos, N. E., Plane turbulent buoyant jets. Part 2. Turbulence structure. *Journal of Fluid Mechanics*, 1977, **81**, 45–62.
5. Chevray, R. and Tutu, N. K., Intermittency and preferential transport of heat in a round jet. *Journal of Fluid Mechanics*, 1978, **88**, 133–160.
6. Dibble, R. W., Kollmann, W. and Schefer, R. W., Conserved scalar fluxes measured in a turbulent nonpremixed flame by combined laser Doppler velocimetry and laser Raman scattering. *Combustion and Flame*, 1984, **55**, 307–321.
7. Owen, F. K., Simultaneous laser measurements of instantaneous velocity and concentration in turbulent mixing flows. *AGARD Conference Proceedings*, Vol. 193, 1976, pp. 27.1–27.7.
8. Papanicolaou, P. N. and List, E. J., Investigation of round vertical turbulent buoyant jets. *Journal of Fluid Mechanics*, 1988, **195**, 341–391.
9. Lemoine, F., Wolff, M. and Lebouché, M., Simultaneous concentration and velocity measurements using combined laser-induced fluorescence and laser Doppler vel-

ocimetry: application to turbulent transport, *Experiments in Fluids*, 1996, **20**, 178–188.
10. Gad-el-Hak, M. and Morton, J. B., Experiments on the diffusion of smoke in isotropic turbulent flow. *AIAA Journal*, 1979, **17**, 558–562.
11. Simoens, S. and Ayrault, M., Concentration flux of a scalar quantity in turbulent flows. *Experiments in Fluids*, 1994, **16**, 273–281.
12. Nakamura, I., Sakai, Y. and Miyata, M., Diffusion of matter by a non-buoyant plume in grid-generated turbulence. *Journal of Fluid Mechanics*, 1987, **178**, 379–403.
13. Walker, D. A., A fluorescence technique for measurement of concentration in mixing liquids. *Journal of Physics E: Scientific Instruments*, 1987, **20**, 217–224.
14. Arcoumanis, C., McGuirk, J. J. and Palma, J. M. L. M., On the use of fluorescent dyes for concentration measurements in water flows, technical notes. *Experiments in Fluids*, 1990, **10**, 177–180.
15. Kistler, A. L. and Vrebalovich, T., Grid turbulence at large Reynolds numbers. *Journal of Fluid Mechanics*, 1996, **26**, 37–47.
16. Comte-Bellot, G. and Corrsin, S., The use of a contraction to improve the isotropy of grid generated turbulence. *Journal of Fluid Mechanics*, 1966, **25**, 657–682.
17. Davies, J. T., *Turbulence Phenomena*. Academic Press, New York, 1972.
18. Launder, B. E., On the effect of gravitational field on the turbulent transport of heat and momentum. *Journal of Fluid Mechanics*, 1975, **67**, 569–581.
19. Everitt, K. W. and Robins, A. G., The development and structure of turbulent plane jets. *Journal of Fluid Mechanics*, 1978, **88**, 563–583.
20. Max, J., *Methodes et Techniques de Traitement du Signal et Applications aux Mesures Physiques*. Masson & Cie, Paris, 1972.